PHYSICAL REVIEW B **70**, 201201(R) (2004)

Large crystal local-field effects in the dynamical structure factor of rutile TiO_2

I. G. Gurtubay,[1] Wei Ku,[2] J. M. Pitarke,[1,3] A. G. Eguiluz,[4,5] B. C. Larson,[5] J. Tischler,[5] and P. Zschack[6]

[1]*Materia Kondentsatuaren Fisika Saila, Zientzi Fakultatea, Euskal Herriko Unibertsitatea, 644 Posta kutxatila, E-48080 Bilbo, Basque Country, Spain*

[2]*Department of Physics, Brookhaven National Laboratory, Bldg. 510, Upton, New York 11973-5000, USA*

[3]*Donostia International Physics Center (DIPC) and Unidad Física Materiales CSIC-UPV/EHU, Manuel de Lardizabal Pasealekua, E-20018 Donostia, Basque Country, Spain*

[4]*Department of Physics and Astronomy, The University of Tennessee, Knoxville, Tennessee 37996-1200, USA*

[5]*Condensed Matter Sciences Division, Oak Ridge National Laboratory, Oak Ridge, Tennessee 37831-6030, USA*

[6]*Frederick Seitz Materials Research Laboratory, University of Illinois, Urbana-Champaign, Illinois 61801, USA*

(Received 3 July 2004; revised manuscript received 15 September 2004; published 2 November 2004)

We present *ab initio* time-dependent density-functional calculations and nonresonant inelastic x-ray scattering measurements of the dynamical structure factor of rutile TiO_2. Our calculations are in good agreement with experiment and prove the presence of large crystal local-field effects below the Ti *M* edge, which yield a sharp loss peak at 14 eV whose intensity features a remarkable nonmonotonic dependence on the wave vector. These effects, which impact the excitation spectra in the oxide more dramatically than in transition metals, provide a signature of the underlying electronic structure.

DOI: 10.1103/PhysRevB.70.201201 PACS number(s): 78.70.Ck, 71.15.Mb, 71.45.Gm

Titanium dioxide (TiO_2) has been studied extensively for its remarkable electric, magnetic, catalytic, and electrochemical properties. Based on these properties, TiO_2 has been used in a wide variety of technological applications, such as dielectric material for integrated electronics and photocatalyst for the decomposition of organic compounds.[1]

In the last decade, many investigations have been carried out focusing on the structural, electronic, and optical properties of this transition-metal oxide. From the experimental point of view it has been studied by various techniques, such as ultraviolet photoemission,[2,3] x-ray emission,[4] x-ray photoemission,[5,6] Auger-electron,[7] and electron-energy-loss spectroscopies.[8–10] Theoretical investigations of this wide-band-gap semiconductor include *ab initio* calculations of its structural, electronic, and optical properties.[11,12]

Recently, Launay *et al.*[10] have shown evidence of a rutile-phase characteristic peak in the low-energy loss spectra of TiO_2, and Vast *et al.*[13] have investigated the impact of crystal local-field effects (LFE) on the electron-energy-loss spectra of rutile TiO_2. These authors used electron-energy-loss spectroscopy (EELS) to study the low-wave-vector behavior of the energy-loss function of this material. They combined their experimental spectra with *ab initio* calculations and concluded that local-field effects are only relevant at energies above 40 eV, where excitations from the Ti 3*p* semicore levels occur.

In this Rapid Communication, we report *ab initio* time-dependent density-functional (TDDFT) calculations of the dynamical structure factor of rutile TiO_2 at large momentum transfers. We also report nonresonant inelastic x-ray scattering (IXS) measurements, which are suited to study the short-wavelength behavior of this quantity, and we observe large crystal local-field effects at low energies. These effects are absent at the small momentum transfers accessible by EELS (Ref. 13); however, we find that at larger momentum transfers, where inhomogeneities due to localized *d* states can be sampled, crystal local-field effects yield a sharp nonmonotonic loss peak at 14 eV.

Within the first Born approximation, the inelastic scattering cross section for x rays to transfer momentum $\hbar(\boldsymbol{q}+\boldsymbol{G})$ and energy $\hbar\omega$ to a periodic solid is characterized by the dynamical structure factor of the solid:

$$\frac{d^2\sigma}{d\Omega d\omega} = \left(\frac{e^2}{m_e c^2}\right)^2 (\boldsymbol{e}_i \cdot \boldsymbol{e}_f)^2 \left(\frac{\omega_f}{\omega_i}\right) \hbar S(\boldsymbol{q}+\boldsymbol{G},\omega), \qquad (1)$$

where $(\boldsymbol{e}_i, \boldsymbol{e}_f)$ and (ω_i, ω_f) refer to the polarization vector and frequency of the incident and scattered photons, respectively, the wave vector $\boldsymbol{q}$ is in the first Brillouin zone (BZ), and $\boldsymbol{G}$ is a vector of the reciprocal lattice. $S(\boldsymbol{q}+\boldsymbol{G},\omega)$ represents the dynamical structure factor[14]

$$S(\boldsymbol{q}+\boldsymbol{G},\omega) = -2\Omega \,\mathrm{Im}\, \chi_{\boldsymbol{G},\boldsymbol{G}}(\boldsymbol{q},\omega). \qquad (2)$$

Here, $\chi_{\boldsymbol{G},\boldsymbol{G}'}(\boldsymbol{q},\omega)$ is the density-response function of the solid, and Ω is the normalization volume.

In the framework of TDDFT,[15] the *exact* density-response matrix of a periodic solid of electron density $n_0(\boldsymbol{r})$ can be written as

$$\chi_{\boldsymbol{G},\boldsymbol{G}'}(\boldsymbol{q},\omega) = \chi^S_{\boldsymbol{G},\boldsymbol{G}'}(\boldsymbol{q},\omega) + \sum_{\boldsymbol{G}_1,\boldsymbol{G}_2} \chi^S_{\boldsymbol{G},\boldsymbol{G}_1}(\boldsymbol{q},\omega)\{v_{\boldsymbol{G}_1}(\boldsymbol{q}) + f^{\mathrm{XC}}_{\boldsymbol{G}_1,\boldsymbol{G}_2}[n_0](\boldsymbol{q},\omega)\}\chi_{\boldsymbol{G}_2,\boldsymbol{G}'}(\boldsymbol{q},\omega). \qquad (3)$$

Here, $f^{\mathrm{XC}}_{\boldsymbol{G},\boldsymbol{G}'}[n](\boldsymbol{q},\omega)$ are the Fourier coefficients of the functional derivative of the time-dependent exchange-correlation (XC) potential of TDDFT, and $\chi^S_{\boldsymbol{G},\boldsymbol{G}'}(\boldsymbol{q},\omega)$ represents the density-response matrix of noninteracting Kohn-Sham (KS) electrons,[16] which is obtained from the knowledge of the eigenfunctions and eigenvalues of the single-particle Kohn-Sham equation of density-functional theory (DFT).[17,18] We solve this equation self-consistently in the local-density approximation (LDA), with use of the Perdew-Zunger

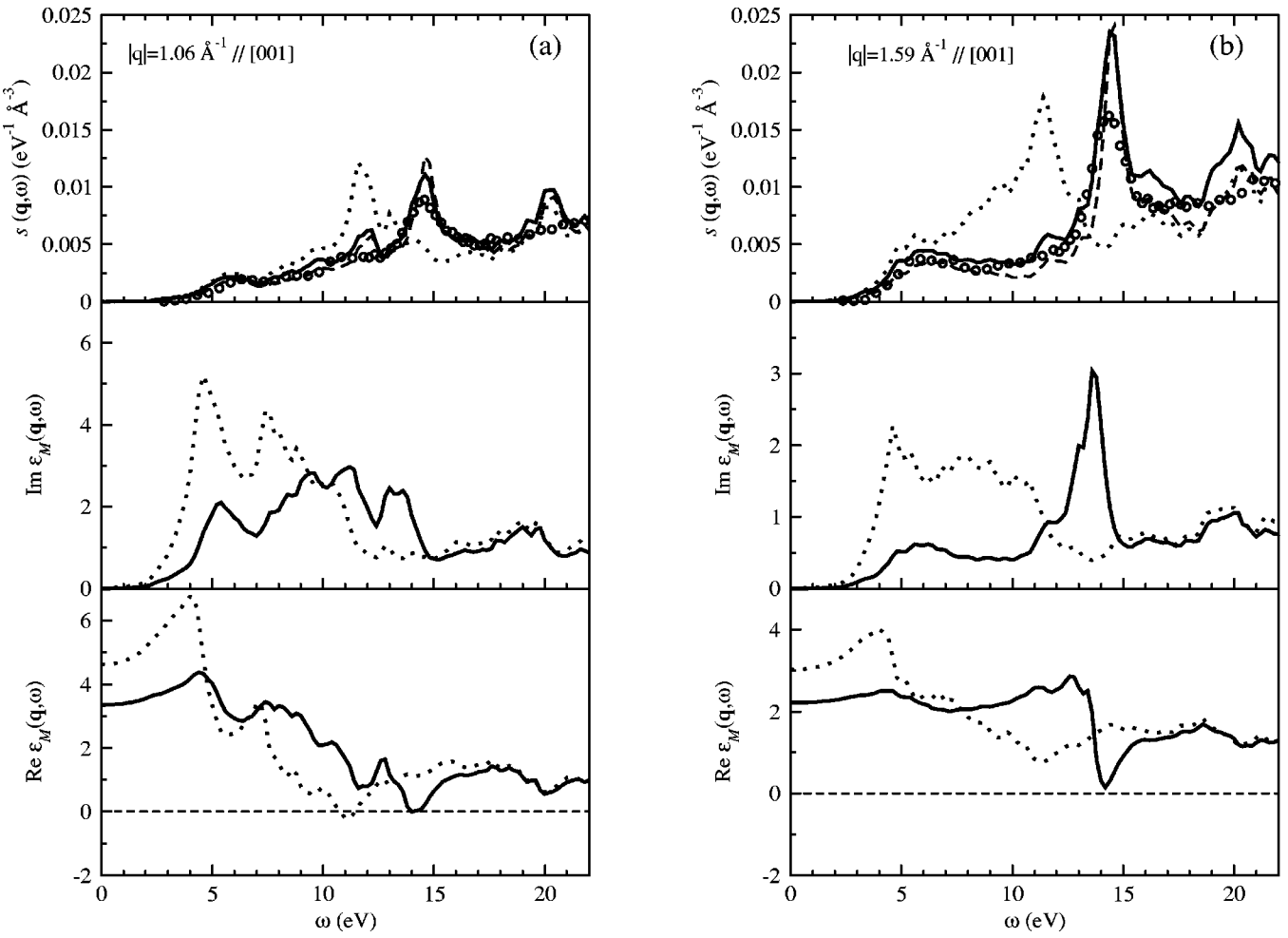

FIG. 1. Dynamical structure factor per unit volume $s(\boldsymbol{q},\omega)$ (top panel) and macroscopic dielectric function $\epsilon_M(\boldsymbol{q},\omega)$ (middle and bottom panels) of TiO_2 at (a) $|\boldsymbol{q}|=1.06$ Å^{-1} and (b) $|\boldsymbol{q}|=1.59$ Å^{-1} along the [001] direction. The solid (dotted) line represents the calculated ALDA spectrum with (without) LFE. The dashed line denotes the calculated RPA result with LFE. Open circles shows the IXS measurements normalized to the same absolute units as the theoretical spectra.

parametrization[19] of the Ceperley-Alder XC energy of a uniform electron gas.[20] In the random-phase approximation (RPA), the XC kernel $f^{\mathrm{XC}}_{\boldsymbol{G},\boldsymbol{G}'}[n](\boldsymbol{q},\omega)$ entering Eq. (3) is taken to be zero; in the so-called adiabatic LDA (ALDA), it is approximated by an adiabatic local kernel of the form

$$f^{\mathrm{XC}}_{\boldsymbol{G},\boldsymbol{G}'}(\boldsymbol{q},\omega)=\int d\boldsymbol{r}\, e^{-i(\boldsymbol{G}-\boldsymbol{G}')\cdot\boldsymbol{r}}\left.\frac{dV_{\mathrm{XC}}(n)}{dn}\right|_{n=n_0(\boldsymbol{r})}, \qquad (4)$$

where $V_{\mathrm{XC}}(n)$ is the XC potential of a homogeneous electron gas of density n.

In the calculations presented below, we first expand the LDA single-particle Bloch states in a linearized augmented plane wave (LAPW) basis,[21] by dividing the unit cell into nonoverlapping atomic spheres and the interstitial region between them. Inside the atomic spheres, the LAPW wave functions are expanded in spherical harmonics with $l_{\max}=10$. The Ti 3*s* and 3*p* states and the O 2*s* states are treated as semicore states, and the Kohn-Sham equation is solved with a cutoff parameter $R_{MT}K_{\max}=8$ and an energy cutoff of 7.5 Ry. The Kohn-Sham density-response matrix has been computed as in Ref. 22, with a damping parameter of 0.2 eV.

Nonresonant inelastic x-ray scattering measurements of the dynamical structure factor of rutile TiO_2 were obtained using the UNICAT undulator Beam Line on the Advanced Photon Source at Argonne National Laboratory. The measurements were made in reflection geometry, with 7.6-keV x rays, a range of wave vectors from 0.5 to 3.98 Å^{-1} in the [001] direction, and an energy resolution of 1.1 eV. The surprising result of these measurements is the nonmonotonic wave-vector dependence of the intensity of a sharp loss peak at 14 eV, which is absent in existing optical ($q=0$) and EELS measurements on this material and whose physics is qualitatively different from the well-known collective excitations in simple metals. Our *ab initio* calculations indicate that this feature is the result of large crystal local-field effects near the plasma frequency.

In order to investigate the impact of crystal local-field effects on the dynamical structure factor of rutile TiO_2, we have first neglected these effects by considering only the diagonal elements of the Kohn-Sham density-response

matrix entering Eq. (3) (diagonal calculation), and we have then solved this matrix equation with a given number of $\boldsymbol{G}$ vectors (full calculation).[23] Well-converged results have been obtained with the matrix size ranging from 63×63 to 113×113, depending on the momentum transfer and the energy range considered, and using 30 points in the irreducible BZ (IBZ).

The energy-loss function $\mathrm{Im}[-\epsilon_{0,0}^{-1}(\boldsymbol{q},\omega)]$ (Ref. 24) of rutile TiO_2 for vanishing momentum transfer (long wavelengths) has been reported by Mo and Ching[12] with no inclusion of crystal local-field effects and more recently by Vast *et al.*[13] with full inclusion of these effects. At small wave vectors, two principal structures can be indentified in the energy-loss function at energies below the titanium *M* edge: a plasmon peak at 12 eV and a broad collective excitation at about 25 eV, stemming from the building up of collective modes of the strongly hybridized Ti 3*d* and O 2*p* bands. Vast *et al.*[13] also reported loss-function calculations of rutile TiO_2 for $|\boldsymbol{q}|\approx0.4$ Å^{-1}, showing that at these small wave vectors crystal local-field effects have little impact at energies below the titanium *M* edge but drastically reduce the peak heights above the Ti *M* edge.

For vanishing and small momentum transfers our calculations esentially reproduce the calculations reported in Refs. 12,13. Besides, for large wave vectors not addressed before we find large crystal local-field effects, as shown by the dynamical structure factor per unit volume $s(\boldsymbol{q},\omega)=S(\boldsymbol{q},\omega)/\Omega$ of rutile TiO_2 which we plot in Fig. 1 for two values of the wave vector and for energies below the Ti *M* edge. IXS measurements of this quantity are scaled to absolute units by first performing an absolute measurement on Al (with the use of the *f* sum rule) (Ref. 25), and then scaling by the ratio of absorption coefficients for Al and TiO_2. Considering the fact that the comparison between the calculations and measurements is in absolute units, with no adjustable parameters, the agreement between theory and experiment is remarkable.

The top panels of Fig. 1 show that in the absence of crystal local-field effects (dotted lines) a *simple* plasmon peak is present at 12 eV, which is well defined for wave vectors up to a critical value of ≈1.5 Å^{-1} where the plasmon excitation enters the continuum of intraband particle-hole excitations. In the presence of local-field effects (solid lines), this plasmon is still present at $|\boldsymbol{q}|=1.06$ Å^{-1} [see Fig. 1(a)] but it is completely damped at larger wave vectors [see Fig. 1(b)]; in *addition*, a sharp loss peak emerges at 14 eV, which brings our calculated energy-loss function into good agreement with experiment.

We have also carried out calculations and measurements of the dynamical structure factor for larger values of the momentum transfer. We have found that the *new* peak at 14 eV, which only appears at nonzero wave vectors, disappears at surprisingly large wave vectors of the order of 3 Å^{-1} without significant broadening. The oscillator strength of this peak, which is qualitatively different from the collective excitations in simple materials, thus features a remarkable, nonmonotonic dependence on the wave vector.

With the aim of establishing the nature of the large crystal local-field effects that yield the characteristic energy-loss function at 14 eV, we have considered the macroscopic dielectric function $\epsilon_M(\boldsymbol{q},\omega)$, which within the first BZ is

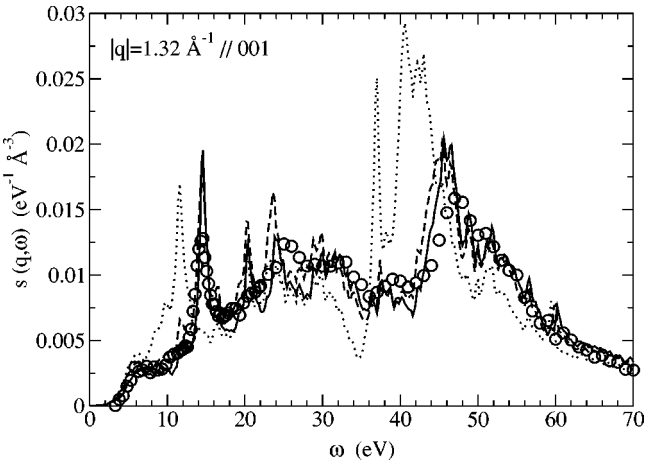

FIG. 2. Dynamical structure factor of TiO_2 at $|\boldsymbol{q}|=1.32$ Å^{-1} along the [001] direction. The solid (dotted) line represents the calculated ALDA spectrum with (without) crystal local-field effects. The dashed line represents the calculated RPA spectrum with crystal local-field effects included. Open circles show the IXS measurements normalized to the same absolute units as the theoretical spectra.

$\epsilon_M(\boldsymbol{q},\omega)=1/\epsilon_{0,0}^{-1}(\boldsymbol{q},\omega)$. Collective excitations occur at energies where both the real and imaginary parts of this dielectric function are close to zero.

The bottom and central panels of Fig. 1 exhibit the real and imaginary parts of $\epsilon_M(\boldsymbol{q},\omega)$. At the smallest wave vectors (not plotted here), crystal local-field effects are small and the real part of the macroscopic dielectric function is zero at 12 eV where the imaginary part is small, thereby yielding a plasmon peak in the corresponding energy-loss function. However, as the wave vector increases, the rapid variation of microscopic electric fields acting on localized *d* states leads to a dramatic redistribution of the strength in the imaginary part of the macroscopic dielectric function (see middle panels of Fig. 1). As a result, collective excitations are considerably damped at 12 eV where Landau damping is now efficient. Instead, a well-defined collective oscillation occurs just above the *new* continuum of particle-hole excitations. Indeed, the Kramers-Kronig relation between the real and imaginary parts of the macroscopic dielectric function guarantees that the real part has a dip whenever the imaginary part has a jump, and the result is a pronounced energy-loss peak (see upper panels of Fig. 1) that is responsible for the realization of a surprisingly sharp collective mode at 14 eV. We have also carried out calculations of the dynamical structure factor of VO_2 (in the rutile structure), which also combines strong inhomogeneities of the Fermi sea with the presence of localized *d* states below and above the Fermi level, and we have found that this material also exhibits a nonmonotonic sharp collective mode at low energies and large momentum transfers.

We close this Rapid Communication with a comparison of ALDA calculations and IXS measurements of the dynamical structure factor of TiO_2 at energies both below and above the Ti *M* edge. Figure 2 represents the results we have obtained for $s(\boldsymbol{q},\omega)$ with $|\boldsymbol{q}|=1.32$ Å^{-1}, showing that when crystal local-field effects are included the overall agreement between theory and experiment is very good.

At low energies below the Ti *M* edge, which is located at ~40 eV, crystal local-field effects yield a well-defined collective excitation at 14 eV, as discussed before. At energies above the Ti *M* edge, a prominent structure is visible, which can be attributed to transitions from the occupied Ti semicore 3*p* states to the lowest conduction bands. In the absence of local-field effects (dotted line), the onset of these transitions would occur at 36 eV. However, local-field effects bring the onset of the *M* edge to ~42 eV and reduces the corresponding peak heights, in close agreement with experiment. Nevertheless, there is still a small mismatch between the converged ALDA calculation and the measured spectrum at the position of the main semicore peak. This mismatch stems from the fact that our calculated LDA ground state exhibits an upper semicore edge that is located a few eV higher than observed experimentally. Figure 2 also shows that many-body XC effects not included in the RPA (dashed line) do not affect the low-energy collective excitation at 14 eV. These effects, however, slightly modify the structure of the collective excitation at ~25 eV [see also Figs. 1(a) and 1(b)] and yield a small shift of the semicore excitation onset and main peak towards lower frequencies.

In summary, we have presented a combined theoretical and experimental investigation of the dynamical structure factor of rutile TiO_2 at large momentum transfers. We have found that large crystal local-field effects in this wide-band-gap semiconductor yield a sharp loss peak at 14 eV. An analysis of the macroscopic dielectric function of this material leads us to the conclusion that this loss peak is originated in a collective excitation which remains present at surprisingly large momentum transfers and whose spectral weight features a remarkable nonmonotonic dependence on the wave vector. This feature is exhibited by both TDDFT calculations and IXS measurements, which show a remarkable agreement when presented in absolute units with no adjustable parameters.

I.G.G. and J.M.P. acknowledge partial support by the Basque Unibertsitate, Hezkuntza eta Ikerketa Saila, the UPV/EHU, and the MCyT. W.K. acknowledges support from the U.S. DOE under Contract No. DE-AC02-98CH10886. A.G.E. acknowledges support from NSF ITR DMR-0219332. ORNL research sponsored by the DOE, Office of Science, DMS under contract with UT-Battelle, LLC; the UNICAT beamline supported by the FS-MRL, ORNL, NIST, and UOP Res.; the Advanced Photon Source (APS) supported by the DOE.

[1] R. Asahi, T. Morikawa, T. Ohwaki, K. Aoki, and Y. Taga, Science **293**, 269 (2001).
[2] R. H. Tait and R. V. Kasowski, Phys. Rev. B **20**, 5178 (1979).
[3] W. Göpel, J. A. Anderson, D. Frankel, M. Jaehnig, K. Phillips, J. A. Schäfer, and G. Rocker, Surf. Sci. **139**, 333 (1984).
[4] K. Tsutsumi, O. Aita, and K. Ichikawa, Phys. Rev. B **15**, 4638 (1977).
[5] A. Carley, P. R. Chalker, J. C. Riviere, and M. W. Roberts, J. Chem. Soc., Faraday Trans. 1 **83**, 351 (1987).
[6] B. W. Veal and A. P. Paulikas, Phys. Rev. B **31**, 5399 (1985).
[7] M. L. Knotek and P. J. Feibelman, Phys. Rev. Lett. **40**, 964 (1978).
[8] R. Brydson, H. Sauer, W. Engel, J. M. Thomas, E. Zeitler, N. Kosugi, and H. Kuroda, J. Phys.: Condens. Matter **1**, 797 (1989).
[9] L. A. Grunes, R. D. Leapman, C. N. Wilker, R. Hoffmann, and A. B. Kunz, Phys. Rev. B **25**, 7157 (1982).
[10] M. Launay, F. Boucher, and P. Moreau, Phys. Rev. B **69**, 035101 (2004).
[11] K. M. Glassford and J. R. Chelikowsky, Phys. Rev. B **46**, 1284 (1992).
[12] S.-D. Mo and W. Y. Ching, Phys. Rev. B **51**, 13023 (1995).
[13] N. Vast, L. Reining, V. Olevano, P. Schattschneider, and B. Jouffrey, Phys. Rev. Lett. **88**, 037601 (2002).
[14] *The Theory of Quantum Liquids*, edited by D. Pines and P. Nozieres (Benjamin, New York, 1996).
[15] M. Petersilka, U. J. Gossmann, and E. K. U. Gross, Phys. Rev. Lett. **76**, 1212 (1996).
[16] A. G. Eguiluz, A. Fleszar, and J. A. Gaspar, Nucl. Instrum. Methods Phys. Res. B **96**, 550 (1995).
[17] P. Hohenberg and W. Kohn, Phys. Rev. **136**, B864 (1964).
[18] W. Kohn and L. Sham, Phys. Rev. **140**, A11333 (1965).
[19] J. P. Perdew and A. Zunger, Phys. Rev. B **23**, 5048 (1981).
[20] D. M. Ceperley and B. J. Alder, Phys. Rev. Lett. **45**, 566 (1980).
[21] P. Blaha, K. Schwarz, and J. Luitz, Computer Code WIEN97.8, Technical University of Vienna, 1997.
[22] W. Ku, W. E. Pickett, R. T. Scalettar, and A. G. Eguiluz, Phys. Rev. Lett. **88**, 057001 (2002).
[23] Crystal local-field effects arise because the microscopic electric field varies rapidly over the unit cell. As a result, the polarization due to an external perturbation will in general contain rapidly varying terms with wave vector $\boldsymbol{q}+\boldsymbol{G}$, which are described by the off-diagonal elements of the dielectric matrix [see S. L. Adler, Phys. Rev. **126**, 413 (1962)].
[24] The inverse dielectric matrix $\epsilon^{-1}_{0,0}(\boldsymbol{q},\omega)$ is obtained from $\epsilon^{-1}_{\boldsymbol{G},\boldsymbol{G}'}(\boldsymbol{q},\omega)=1+4\pi/(\boldsymbol{q}+\boldsymbol{G})^2\chi_{\boldsymbol{G},\boldsymbol{G}'}(\boldsymbol{q},\omega)$.
[25] J. Z. Tischler, B. C. Larson, P. Zschack, A. Fleszar, and A. G. Eguiluz, Phys. Status Solidi B **237**, 280 (2003).